JOURNAL OF APPLIED ELECTROCHEMISTRY 19 (1989) 183–187

Computation of primary current distribution and cell resistance at model electrodes with circular perforations

KOICHI AOKI

Department of Electronic Chemistry, Graduate School At Nagatsuta, Tokyo Institute of Technology, Nagatsuta, Midori-ku, Yokohama, 227 Japan

YOSHINORI NISHIKI

Research and Development Center, Permelec Electrode Ltd, 1159, Ishikawa, Fujisawa, 252 Japan

Received 25 January 1988; revised 16 May 1988

A model of a gas-evolving production-type cell with a circularly perforated anode is described. A unit of the model was composed of a disk cathode, a separator and a ring anode in turn. These were located in a cylindrical cell filled with solution. Primary current and potential distributions in the unit cell were computed by solving the Laplace equation in cylindrical coordinates by the finite element method. Geometric parameters determining the distributions were primarily the interelectrode distance and the percentage open area. Current distribution in the open part was larger than that in a rectangular cell with the same geometric parameters because of the cylindrically concentrated supply of the current from the inner part of the ring and the back side of the anode. The unit cell resistance was evaluated as a function of the geometric parameters. It exhibited a linear variation of the interelectrode distance and the square of the percentage open area. There was, however, a slight dependence of the percentage open area on the unit cell resistance and hence it is concluded that circularly perforated electrodes provide higher performance than louvre-type electrodes.

Nomenclature

d_1	distance between the front side of the anode and the separator
d_2	thickness of the separator
H	height of the anode on a large scale
I	total current in the unit cell
i	current density
p	pitch, i.e. diameter of the cylindrical unit cell
R	unit cell resistance, defined by Equation 13
R_t	total cell resistance in a cell on a large scale
r	radial length in the cylindrical coordinate
s	superficial surface area, given by Equation 2
t	thickness of the anode
v	test function
W	width of the anode in a cell on a large scale
w	width of the anode of the unit cell
z	axial length in the cylindrical coordinate
dy	infinitesimal length on the boundary
ϱ	resistivity
ϕ	potential
ϕ^*	potential at the anode
Γ	linear integration contour
Ω	double integration space
ν	length normal to the boundary

Subscripts

a	anode
c	cathode
cy	cylindrical model
rc	rectangular model
1	solution phase
2	separator phase

1. Introduction

Evaluation of the current and the potential distributions in electrolytic cells is a classical electrochemical problem and involves solution of the Laplace equation. The most basic work on this subject is the determination of the distribution in a rectangular cell involving the point-plane and the line-plane electrodes by Kasper [1]. Since his pioneering work, the mathematical approach for the distribution has been directed to various kinds of model cells with more complicated geometries [2–5]. It has been extended to systems associated with overpotential [2–6], arrangement of current feeders for resistive electrodes [4, 7–11] and gas evolution [6, 12]. Most of these theoretical works have employed the Fourier transformation or the Schwarz–Christoffel transformation. The former is powerful for analysis in a cell with three-dimensional rectangular enclosures, whereas the latter is helpful for calculation in a two-dimensional polygonal cell. Evaluation of the distribution in more complicated cell geometries has to rely upon numerical computation [13] such as the finite element method and the boundary element method. Since numerical methods rarely suffer because of geometrical complications [14] or intricate boundary conditions, they

0021-891X/89 $03.00 + .12

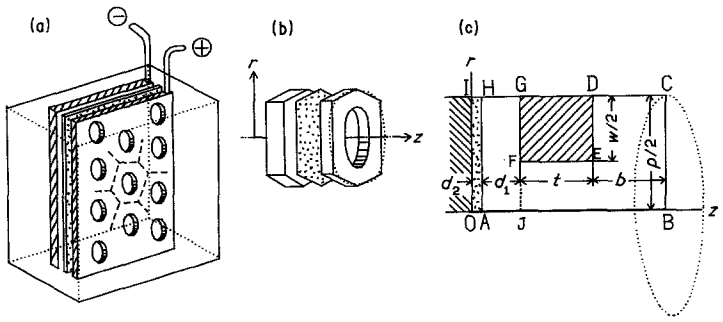

Fig. 1. (a) Model cell composed of an anode with circular perforations, a plate cathode (hatched lines) and a membrane (a dotted plate). (b) Hexagonal unit cell extracted from the model cell. The hexagon is approximated as a cylinder (dotted curve in b). (c) A half cross section of the cylindrical model cell. Revolution of DEFG around the z-axis yields a unit anode.

can be applied directly to computation in real cells by introducing a number of system parameters [15]. However, there is the possibility of missing a systematic variation inherent to a given parameter.

To specify the effects of electrode geometry employed for industrial electrolysis on the current distribution and cell voltage, we have introduced a rectangular model for an electrode with open parts through which evolving gas is removed from the inter-electrode space [16]. We have further obtained cell resistances for the cases of the primary [16] and the secondary [17] current distributions and those of the gas-evolving electrode [18]. A significant conclusion of these studies is that the unit cell resistance increases with increase in the size of the open part. This effect of the open size has been experimentally examined at louvred, circularly perforated and flattened mesh electrodes [19]. Unfortunately, these electrode geometries, especially the circularly perforated electrode, are not reasonably represented by rectangular models that have been presented previously [14]. In this paper, we introduce a cylindrical model for the circularly perforated electrode and evaluate the cell resistance due to the primary current distribution by the finite element method.

2. Model cell

Figure 1a illustrates a cell composed of a circularly perforated anode and a cathode plate, between which a separator or a membrane with uniform resistivity is mounted. It is assumed that the anode and the cathode are so conductive that a potential gradient does not occur in the electrodes. Since our concern is the current distribution in the vicinity of the anode or in the anolyte, we represent the series connections of resistance of the catholyte and the membrane by the equivalent resistance of the membrane. Thus the cathode is connected to adhere closely to the membrane in this model cell. When circularly perforated openings are arranged in a rigid hexagonal array, a hexagon can be regarded as a model unit cell, as illustrated in Fig. 1b. If the hexagonal unit is approximated by a circular cylinder as shown by a dotted curve in Fig. 1b, it corresponds to a revolution of the two-dimensional rectangular cell in Fig. 1c, by taking the axis to be OB. A similar approximation has been used for the effects of attached bubbles on current distribution [20].

Significant geometric parameters for this model are the percentage open area, o_p, and the superficial surface area, s, defined, respectively, as

$$o_p = 100\,\frac{\pi[(p-w)/2]^2}{\pi(p/2)^2} = 100[(p-w)/p]^2 \quad (1)$$

$$s = \frac{2\pi\{(p/2)^2 - [(p-w)/2]^2\} + \pi(p-w)t}{\pi(p/2)^2} = \frac{2w(2p-w) + 4(p-w)t}{p^2} \quad (2)$$

This open area ratio ($o_p/100$) is the square of that for the rectangular model. The superficial surface area is close to that for the rectangular model when o_p and t are small. Conversely, for large values of o_p, it becomes twice the superficial surface area of the rectangular model.

3. Computation of current distribution

It is asumed that the solution has uniform resistivity over the phase. Then the potential, ϕ, is expressed by the Laplace equation in cylindrical coordinates both in the solution and the membrane phases

$$\partial^2\phi/\partial r^2 + (1/r)(\partial\phi/\partial r) + \partial^2\phi/\partial z^2 = 0 \quad (3)$$

The following boundary conditions are used. The potentials at the anode and the cathode are taken to be ϕ^* and 0, respectively. At the boundary between the cathode and the membrane the potential is continuous across both phases, and the current densities on both sides of the boundary are identical, i.e. on the side AH

$$\phi_2 = \phi_1 \quad (4)$$

$$(\partial\phi_1/\partial z)\varrho_1 = (\partial\phi_2/\partial z)/\varrho_2 \quad (5)$$

On the side of the insulated walls, the potential vanishes.

Multiplying Equation 3 by a test function, v, and $2\pi r$, integrating the resulting equation with respect to r and z over the membrane and the solution phases, and applying Green's theorem yields

$$\int_{\Gamma_{OI}} V_2 d\gamma + \int_{\Gamma_{AH}} V_2 d\gamma + \int\int_{\Omega_2} U\,dr dz = 0 \quad (6)$$

$$\int_{\Gamma_{DEFG}} V_1 d\gamma + \int_{\Gamma_{AH}} V_1 d\gamma + \int\int_{\Omega_1} U\,dr dz = 0 \quad (7)$$

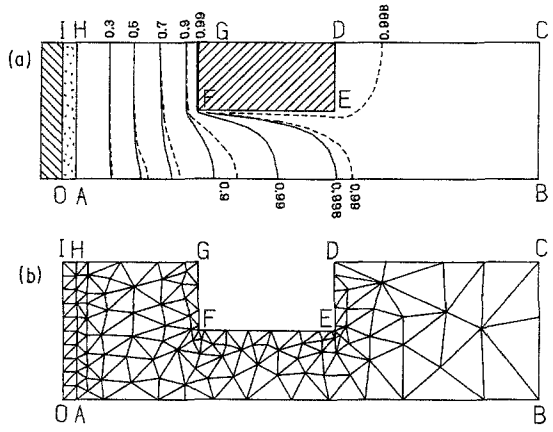

Fig. 2. Equi-potential contours (a) in the cylindrical cell (——) revolved around axis OB and in the rectangular cell (– – –). Digits on the contours denote values of ϕ/ϕ^*, which correspond to an anode potential of 1 and a cathode potential of 0. The contours were computed for the triangularly partitioned unit cell (b) with the following geometrical parameters: $d_1/p = 0.5$, $d_2/p = 0.05$, $w/p = 0.5$, $t/p = 0.5$, $b/p = 0.75$ and $\varrho_2/\varrho_1 = 2.0$.

where

$$V_k = vr(\partial\phi_k/\partial v) \qquad (k = 1, 2) \tag{8}$$

$$U = r[(\partial v/\partial r)(\partial\phi/\partial r) + (\partial v/\partial z)(\partial\phi/\partial z)] \tag{9}$$

Multiplying Equations 6 and 7 by ϱ_1 and ϱ_2, respectively, and adding them by the use of Equation 5 leads to

$$\varrho_2 \int_{\Gamma_{DEFG}} V_1 \mathrm{d}\gamma + \varrho_1 \int_{\Gamma_{OI}} V_2 \mathrm{d}\gamma = \varrho_2 \int\int_{\Omega_1} U \,\mathrm{d}r\mathrm{d}z + \varrho_1 \int\int_{\Omega_2} U \,\mathrm{d}r\mathrm{d}z \tag{10}$$

Equation 10 has a form facilitating computation using the finite element method. The integrals in Equation 10 were rewritten as matrices [21] by using the simplest linear functions at triangular elements. The numbers of nodes and elements were 150–200 and 250–300, respectively. The resulting matrices were a set of simultaneous linear equations for ϕ. Unknown values of ϕ were determined using a 16-bit personal computer, PC9801 (NEC, Tokyo). The computation time was 10–20 s at each cell geometry.

The current density at the anode, i_a, is expressed by

$$i_a = (\partial\phi_1/\partial v)/\varrho_1 \tag{11}$$

on DEFG. The total current at the anode is given by

$$I_a = (2\pi/\varrho_1) \int_{\Gamma_{DEFG}} vr(\partial\phi_1/\partial v)\mathrm{d}\gamma \tag{12}$$

4. Current and potential distributions

Figure 2a shows equi-potential contours computed by the finite element method for an assembly of triangular elements as illustrated in Fig. 2b. Equi-potential contours in the domain AFGH are almost parallel to AH and exhibit linear potential gradients. In the other domain of the solution phase, they are curved owing to the open part of the anode. Of interest is comparison of the contours in the cylindrical cell (——) with those in the rectangular one (– – –). The potential gradient in the domain ABF of

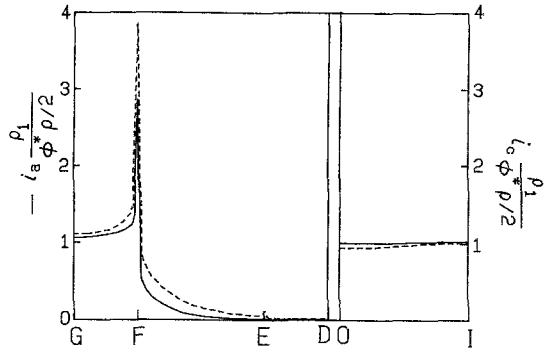

Fig. 3. Distributions of dimensionless current density at the anode and the cathode in the cylindrical cell (——) and the rectangular cell (– – –) with the same geometry as in Fig. 2.

the cylindrical cell is larger than in the rectangular one. This fact is ascribed to concentration of the current into the open part from the cylindrical side, EF.

Figure 3 shows distribution of the dimensionless current densities at the anode (i_a) and at the cathode (i_c). As expected from Fig. 2a, the current density at the cathode is distributed uniformly. It is, however, non-uniform when d_1 is small without the membrane, as has been shown in Fig. 3 of Ref. [14]. The cathode current density near the open part or at the left of OI in the cylindrical cell (——) is slightly larger than that in the rectangular cell (– – –) because of a cylindrically concentrated supply of the current from sides EF and DE. On the other hand, the current density at the anode is non-uniform, and especially the current density at F is infinite for primary current distribution because of the acute edge. The anode current density in the cylindrical cell is smaller than that in the rectangular one. This can be explained by the value of the superficial surface area in the cylindrical cell ($s = 2.5$) being larger than that for the rectangular one ($s = 2.0$). Apparent inconsistency that $i_{c,cy} > i_{c,rc}$ regardless of $-i_{a,cy} < -i_{a,rc}$ is ascribed to $s_{cy} > s_{rc}$ or the large ratio of the cylindrical anode area to the rectangular anode area. The ratio, $i_{a,cy}/i_{a,rc}$, decreases with increase in the distance from the point F.

We obtained partitions of the total current into the currents on the three sides, DE, EF and FG, and plotted them against o_p for $\varrho_2/\varrho_1 = 1$ (——) and 100 (· · · ·) in Fig. 4 for small values of $d_1(p/2)$. With an increase in ϱ_2/ϱ_1, the partition on side FG decreases because the current distribution in the membrane becomes uniform. Variations of the partitions with o_p were linear for the EF and FG sides and had slight dependence on the superficial surface area for $1.7 < s < 2.5$. These trends have also been observed in the rectangular cell (e.g. in Fig. 5 of Ref. [14]) when $s \geqq 1.7$. For large values of s, the linear relation between o_p and the partitions may hold generally because most of the current through FJ in Fig. 1c is attributed to side EF. Figure 4 also shows the partition for the rectangular cell $\varrho_2/\varrho_1 = 1$ (– – –) and 100 (–·–·–·–). The partition on side EF in the cylindrical cell is larger than that in the rectangular cell at the same value of ϱ_2/ϱ_1. However, dependence of the

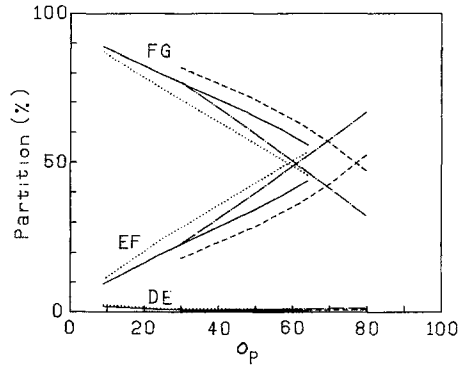

Fig. 4. Partition of the total currents into the three sides of DE, EF and FG at $s = 2.0$ in the cylindrical model at $\varrho_2/\varrho_1 = 1$ (——) and 100 (· · · ·) and the two-dimensional rectangular model at $\varrho_2/\varrho_1 = 1$ (– – –) and 100 (–·–·–·–) when $d_1/p = d_2/p = 20$. It is worthwhile to note that the pattern of the cross section for the cylindrical model is different from that for the rectangular one in spite of a common value of s.

partitions on ϱ_2/ϱ_1 in the cylindrical cell is less than that in the rectangular one.

5. Unit cell resistance

The unit cell resistance, R, is defined by

$$R = \phi^*/I \tag{13}$$

In Fig. 5, the dimensionless unit cell resistance, $R(p/2)/\varrho_1$, is plotted against o_p in cells without (a–e) and with (f–i) the membrane for various combinations of d_1, d_2 and ϱ_2/ϱ_1. Curves g and h are very similar to d and e, respectively, indicating that the resistance of the interelectrode gap can be represented by the series connection of the resistance of the membrane and that of the solution in the interelectrode domain. Variations of the resistance with o_p are much smaller than those for the rectangular cell (see Fig. 4 of Ref. [14]). The minor effect of the o_p on the resistance suggests that the open part with the radius FJ in Fig. 1c might play the same role in electrolysis as the ring anode, FG. In other words, the cylindrical side EF supplies the current to the open part as if side FJ were a uniform current source. Therefore, the perforation does not appreciably increase the cell resistance, but

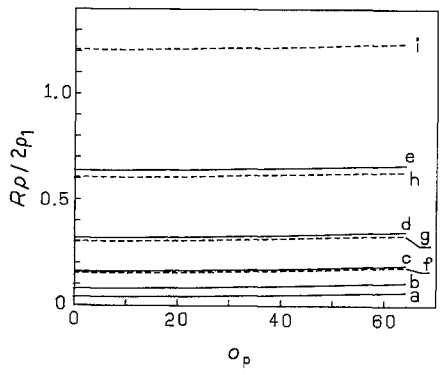

Fig. 5. Variations of unit cell resistance with the percentage open area for $s = 2.0$ in the cell without membrane (a–e) at $d_1/(p/2) =$ (a) 0.125, (b) 0.25, (c) 0.5, (d) 1.0 and (e) 2.0. Curves f–i are in the cell with the membrane having $\varrho_2/\varrho_1 = 10$ at $(d_1/(p/2), d_2/(p/2)) =$ (f) (0.225, 0.025), (g) (0.45, 0.05), (h) (0.9, 0.1) and (i) (1.8, 0.2).

does promote removal of evolving gases out of the interelectrode region.

In order to examine quantitatively the effect of the open part, we derived a simple approximate equation for the unit cell resistance, which is given by

$$R = (\varrho_1 d_1 + \varrho_2 d_2)/\{\pi(p/2)^2\} + 0.065(o_p/100)^2\varrho_1/(p/2) \tag{14}$$

This equation has errors less than 3% for $o_p < 64\%$ and $d_1/p > 0.1$. These conditions are in the available domain for conventional perforation. In the rectangular cell, the coefficient in the second term is 0.33 instead of 0.065. The smaller value for the cylindrical model indicates that the effect of the perforated open part on the resistance is only one-fifth of that in the rectangular cell.

6. Effect of pitch on total cell resistance

In a large-scale industrial cell, which may be regarded as an assembly of many rectangular unit cells, the resistance in large cells with a louvre-type electrode decreases with decreasing pitch [19]. It has been theoretically demonstrated that decreasing the pitch leads to a decrease in the cell resistance [16]. We attempted to examine whether this relation is also applicable to large-scale perforated electrodes. Rigidly assembling the polygonal unit cells so that the height and width of the anode are H and W, respectively, gives the expression for the cell resistance on a large scale

$$R_t = \pi R(p/2)^2/(HW) = \{\varrho_1 d_1 + \varrho_2 d_2 + 0.10(o_p/100)^2\varrho_1 p\}/(HW) \tag{15}$$

The dependence of R_t on p is three-fifths as much as that for the rectangular model. Therefore, making the unit cell small decreases linearly the total cell resistance. This finding has been demonstrated experimentally in Fig. 5 of Ref. [17].

7. Conclusion

A loss of the front part (corresponding to FG side) of the electrode due to the perforation is compensated by a supply of the current from the cylindrical side EF. Therefore the increase in the unit cell resistance due to the perforation is not significant, suggesting that the perforation would raise performance of the cell since it promotes removal of gas bubbles. This is not the case for the rectangular model cell exemplified by a louvre-type electrode. Thus, circularly perforated electrodes provide higher performance than louvre-type electrodes from the viewpoint of cell voltage when compared with cells having the same values of o_p and s. When constructing a perforated electrode, we encounter the question of which is a higher performance electrode — one with a large number of small openings or one with a small number of large openings. The former provides higher performance so

long as only the primary current distribution is concerned.

References

[1] C. Kasper, *Trans. Am. Electrochem. soc.* **78** (1940) 131, 147; **82** (1942) 152.
[2] S. Ishizaka and H. Matsuda, *Denkikagaku* **19** (1951) 89.
[3] H. Matsuda and S. Ishizaka, *Denkikagaku* **20** (1952) 38, 84.
[4] S. Ishizaka, H. Matsuda and Y. Wada, *Denkikagaku* **22** (1954) 420.
[5] C. Wagner, *J. Electrochem. Soc.* **98** (1951(116; 99 (1952) 1.
[6] C. W. Tobias, *J. Electrochem. Soc.* **106** (1959) 833.
[7] S. Komagata, *Denki Shikenjo Kenkyu Houkoku* No. 294 (1930).
[8] C. W. Tobias and R. Wijman, *J. Electrochem. Soc.* **100** (1953) 459.
[9] P. Robertson, *Electrochim. Acta* **22** (1977) 411.
[10] Y. Nishiki, K. Aoki, K. Tokuda and H. Matsuda, *J. Appl. Electrochem.* **17** (1987) 445.
[11] K. Aoki, Y. Nishiki, K. Tokuda and H. Matsuda, *J. Appl. Electrochem.* **17** (1987) 552.
[12] Y. Nishiki, K. Aoki, K. Tokuda and H. Matsuda, *J. Appl. Electrochem.* **16** (1986) 615.
[13] G. A. Prentice and C. W. Tobias, *J. Electrochem. Soc.* **129** (1982) 72.
[14] A. D. Martin, A. A. Wragg and J. C. R. Turner, *Inst. Chem. Eng. Symp. Ser.* **98** (1986) 38.
[15] A number of reports have been presented, especially for mass transport in cells. For example, I. Rousar, V. Cezner, J. Nejepsova, M. M. Jacksic, M. Spasojevic and B. Z. Nikolic, *J. Appl. Electrochem.* **7** (1977) 427.
[16] Y. Nishiki, K. Aoki, K. Tokuda and H. Matsuda, *J. Appl. Electrochem.* **14** (1984) 653.
[17] Y. Nishiki, K. Aoki, K. Tokuda and H. Matsuda, *J. Appl. Electrochem.* **16** (1986) 291.
[18] Y. Nishiki, K. Aoki, K. Tokuda and H. Matsuda, *J. Appl. Electrochem* **17** (1987) 67.
[19] Y. Nishiki, S. Nakamatsu, K. Aoki and K. Tokuda, *J. Electrochem. Soc.* **19** (1989) 90.
[20] J. Dukovic and C. W. Tobias, *J. Electrochem. Soc.* **134** (1987) 331.
[21] O. C. Zienkiewich, 'The Finite Element Method', McGraw-Hill, London (1977).